

Empirical Valence Bond Simulations Suggest a Direct Hydride Transfer Mechanism for Human Diamine Oxidase

Aleksandra Maršavelski,^{†,‡,§,||} Dušan Petrović,^{§,||} Paul Bauer,^{§,||} Robert Vianello,^{*,†,||} and Shina Caroline Lynn Kamerlin^{*,§,||}

[†]Computational Organic Chemistry and Biochemistry Group, Division of Organic Chemistry and Biochemistry, Ruđer Bošković Institute, Bijenička cesta 54, 10000 Zagreb, Croatia

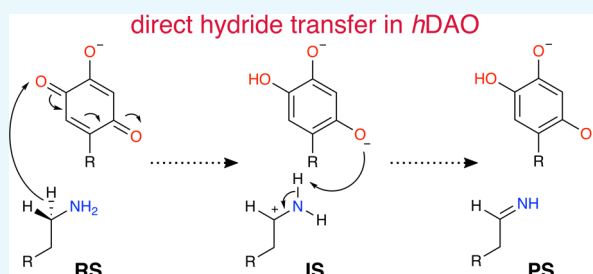
[‡]Department of Chemistry, Faculty of Science, University of Zagreb, Horvatovac 102a, 10000 Zagreb, Croatia

[§]Department of Cell and Molecular Biology, Uppsala University, BMC Box 596, S-751 24 Uppsala, Sweden

^{||}Department of Biophysics, SciLifeLab, KTH Royal Institute of Technology, S-10691 Stockholm, Sweden

S Supporting Information

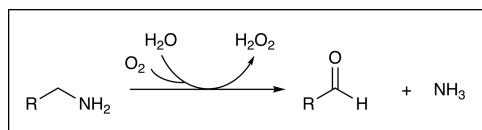
ABSTRACT: Diamine oxidase (DAO) is an enzyme involved in the regulation of cell proliferation and the immune response. This enzyme performs oxidative deamination in the catabolism of biogenic amines, including, among others, histamine, putrescine, spermidine, and spermine. The mechanistic details underlying the reductive half-reaction of the DAO-catalyzed oxidative deamination which leads to the reduced enzyme cofactor and the aldehyde product are, however, still under debate. The catalytic mechanism was proposed to involve a prototropic shift from the substrate–Schiff base to the product–Schiff base, which includes the rate-limiting cleavage of the C α –H bond by the conserved catalytic aspartate. Our detailed mechanistic study, performed using a combined quantum chemical cluster approach with empirical valence bond simulations, suggests that the rate-limiting cleavage of the C α –H bond involves direct hydride transfer to the topaquinone cofactor—a mechanism that does not involve the formation of a Schiff base. Additional investigation of the D373E and D373N variants supported the hypothesis that the conserved catalytic aspartate is indeed essential for the reaction; however, it does not appear to serve as the catalytic base, as previously suggested. Rather, the electrostatic contributions of the most significant residues (including D373), together with the proximity of the Cu²⁺ cation to the reaction site, lower the activation barrier to drive the chemical reaction.



INTRODUCTION

Amine oxidases (AOs) are a group of enzymes that catalyze the degradation of amines into the corresponding aldehydes with the concomitant production of hydrogen peroxide and ammonia, as shown in Scheme 1. They are divided into two

Scheme 1. General Reaction of AOs



structurally distinct classes of enzymes, depending on the cofactor involved in the oxidative deamination reaction:^{1–3} (i) the copper-containing AOs [e.g., diamine oxidase (DAO)], and (ii) the flavin adenine dinucleotide-containing AOs [e.g., monoamine oxidase B (MAO B)]. Both DAO and MAO B are involved in histamine degradation in the human body⁴ and are thus crucial for the regulation of histamine at physiological concentrations.

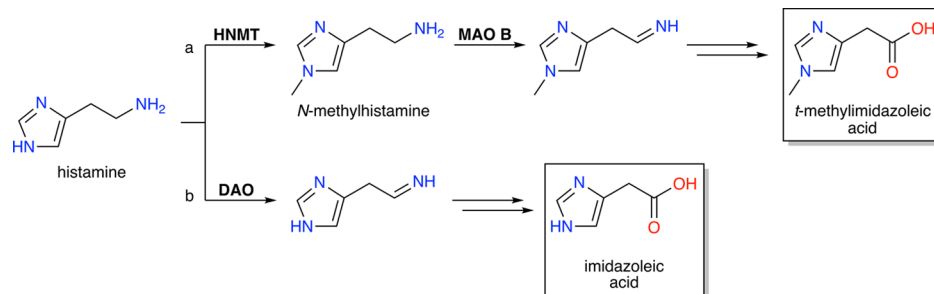
In the central nervous system, histamine degradation is initiated by its methylation with histamine *N*-methyltransferase (HNMT), producing *N*-methylhistamine, which is inactive at the histamine receptor sites and which is further oxidized by MAO B to the corresponding imine. The imine leaves MAO B and undergoes non-enzymatic hydrolysis to the respective aldehyde,^{5,6} which is rapidly further metabolized by aldehyde dehydrogenase to *t*-methyl-imidazoleacetic acid (Scheme 2a).⁷ In contrast, in peripheral tissues, DAO acts directly on histamine (Scheme 2b), yielding imidazoleacetic acid as the end product of histamine degradation.⁷ Because of its broad substrate specificity, including activity toward histamine-related compounds such as *N*-methylhistamine,⁸ and others like cadaverine (1,5-diaminopentane),⁹ putrescine (1,4-diaminobutane),⁸ and the polyamine spermidine,⁸ DAO is a frontline enzyme for the degradation of exogenous amines. Hence, reduced levels of both DAO activity and expression have been directly linked to histamine intolerance.⁴ This, in turn, leads to

Received: February 26, 2018

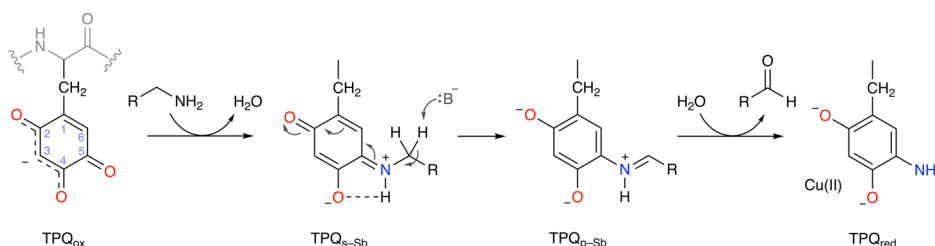
Accepted: March 19, 2018

Published: April 2, 2018

Scheme 2. Pathways for the Degradation of Histidine by the Enzymes: (a) MAO B and (b) DAO



Scheme 3. Proposed Mechanism for the Copper AO Catalyzed Oxidative Deamination of Amines, Adapted from Ref 16



numerous unpleasant symptoms, including, for example, diarrhea, headaches, nasal congestion, asthmatoïd wheezing, hypotension, and arrhythmia, as described in ref 4 and references cited therein.

The DAO-catalyzed oxidative deamination consists of reductive and oxidative half-reactions. While the former leads to the reduced enzyme cofactor and the aldehyde product,¹⁰ the latter involves the reoxidation of the enzyme cofactor by molecular oxygen, which produces ammonia and hydrogen peroxide (Scheme 1). Measurements of primary kinetic isotope effects indicated that the rate-limiting step of these reactions is the cleavage of the C α -H bond.¹¹ Oxidation of *p*-dimethylaminomethylbenzylamine and its deuterated analogue by DAO gave k_H/k_D values up to 5.5.¹¹ This led the authors to propose a mechanism that involves the formation of a Schiff-base between the amine group of the substrate and the C5-carbonyl atom of the 2,4,5-trihydroxy phenylalanine-quinone (TPQ) cofactor (Scheme 3). The prototropic shift from the substrate-Schiff base to the product-Schiff base includes the rate-limiting cleavage of the C α -H bond,^{11–14} as postulated in a study where 2-hydroxy-5-*tert*-butyl-1,4-benzoquinone was used as a model for the topaquinone (TPQ) cofactor to study the mechanism of benzylamine oxidation in acetonitrile.¹² According to the proposed mechanism (Scheme 3), benzylamine and the model cofactor (TPQ_{ox}) form a covalent substrate-Schiff base complex (TPQ_{s-Sb}), followed by the base-catalyzed proton abstraction from the substrate-Schiff base complex, resulting in the product-Schiff base complex (TPQ_{p-Sb}). The product-Schiff base complex is finally hydrolyzed to an aldehyde and the aminoresorcinol form of the reduced cofactor (TPQ_{red}). In the enzyme-catalyzed reaction, a conserved aspartate residue was proposed to act as the catalytic base.¹⁵

Extensive mutagenesis studies have indicated that D383 of *Escherichia coli* AO (*ecAO*) is critical for this enzyme's catalytic activity.^{13,14} That is, the D383E variant showed very low, but measurable, activity.¹³ The D383N and D383A variants were inactive, with the former having drastically reduced affinity for the 2-hydrazinopyridine inhibitor, compared to the wild-type

(WT) enzyme.¹⁴ It was, therefore, concluded that D383 performs an essential role in catalysis, acting as the catalytic base, allowing the conversion of a substrate-Schiff to a product-Schiff base complex.

The role of the copper ion has also been extensively studied,^{17,18} indicating its necessity for the catalytic mechanism of these AOs. It was shown that the copper-free form of the pig-kidney AO completely lost its activity.¹⁸ Upon the addition of copper, however, the enzyme activity was fully restored.¹⁸ It was also demonstrated that Ni²⁺ and Zn²⁺ do not bind the protein, whereas Co²⁺ can be incorporated to the same extent as Cu²⁺, but the Co-reconstituted enzyme shows only very modest activity.¹⁸

The present study aims to elucidate the catalytic mechanism of the oxidative deamination of histamine by human DAO (*hDAO*) and to investigate the role of the catalytic D373 residue, which corresponds to D383 in the homologous enzyme *ecAO*. To address these issues, we performed quantum-mechanical (QM) cluster calculations of the enzyme active site,¹⁹ followed by empirical valence bond (EVB)^{20–22} calculations of the full system that allowed us to calculate the reaction free energies. Our calculations show that the rate-limiting step of histamine degradation is the cleavage of the C α -H bond, as previously described.¹¹ However, the reaction proceeds via direct hydride transfer from histamine to the TPQ cofactor, thus ruling out the previously proposed Schiff-base formation. Moreover, studies of the D373E and D373N variants indeed prove that the conserved catalytic aspartate is essential for the reaction, but it does not serve as the catalytic base, as previously proposed.²³ By describing the catalytic mechanism of *hDAO* in detail, we provide a fundamental understanding of this enzyme that is necessary for the design of therapeutics for the treatment of histamine intolerance.^{4,24}

RESULTS AND DISCUSSION

QM Cluster Models. As the starting point of this work, we used QM cluster models of DAO, together with models of the corresponding non-enzymatic reaction, to probe the proposed mechanism of this enzyme through the formation of a

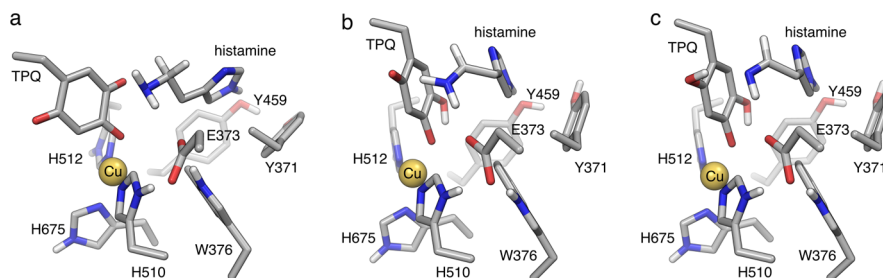


Figure 1. Structures of the (a) reactant, (b) intermediate, and (c) product states for the DAO-catalyzed oxidation of histamine obtained using a QM cluster model to represent the active site of *h*DAO. Nonpolar hydrogen atoms have been omitted for clarity. Rather than annotating (and overcrowding) the figure, the associated key distances are shown in Table S1, and the associated coordinates are also provided in the Supporting Information.

substrate–Schiff base complex.^{12,25} Such models have been used extensively to study enzymatic reaction mechanisms,^{19,26} as well as being the basis of the “theozymes” used for de novo enzyme design purposes.^{27,28} Our initial model systems for the non-enzymatic reaction included (i) histamine and the TPQ cofactor as well as (ii) an extended model including histamine, TPQ, and a Cu^{2+} ion. Both models were optimized at the M11L/6-31G(d) level of theory, with the addition of the SDD basis set for the extended model with copper. Using this approach, it was not possible to obtain an optimized structure for the substrate–Schiff base complex in either the gas phase or continuum solvent [using the conductor-like polarizable continuum model (CPCM),²⁹ with a dielectric constant of 80]. In all attempts to obtain this complex, potential energy surface scanning resulted in quinone-ring opening, which suggests that it is highly unlikely that such a substrate–Schiff base complex exists in the absence of the enzyme.

To examine whether this mechanism is possible in the *h*DAO active site, we created a larger QM cluster model of the enzyme. This model consisted of the histamine substrate, the Cu^{2+} cation, the TPQ cofactor, and the active site residues (i.e., D373, Y371, W376, Y459, H510, H512, and H675), as shown in Figure 1. All amino acid side chains and the TPQ cluster were truncated at the α -atom and capped with methyl groups. The histamine was modeled in its neutral unionized form. Although it has been shown that the substrate binds the active site in its protonated form,³⁰ the substrate needs to be deprotonated to its unionized form to both restore its nucleophilic character and initiate the reaction shown in Scheme 3.^{31,32} Because the physiological pK_a value of histamine is around 9.4, the latter can easily be achieved by active site water molecules with a cost of only a few $\text{kcal}\cdot\text{mol}^{-1}$.³³ In addition, the pK_a of the 4-hydroxyl group of the TPQ cofactor has been suggested to be as low as ~ 3 , which is in part due to its proximity to the catalytic Cu^{2+} ion which will stabilize the charge on the oxyanion and facilitate its deprotonation.³⁴ Therefore, deprotonating the TPQ cofactor in the active site will be facile, and in our simulations, it was modeled as an oxyanion, because this form was shown to exist in the active site even before the reaction occurs.³⁵ The resulting cluster model was embedded into continuum solvent, using the CPCM model with a dielectric constant of 4.

Once the optimized reactant complex was obtained, we performed an energy scan along the distance between the nitrogen atom of the chain amino group of histamine and the C5-carbonyl atom of the TPQ cofactor. As can be seen from Figure S1, it was not possible to locate a transition state along this reaction coordinate. We therefore examined other

mechanistic possibilities. Our previous computational work on the related enzyme, MAO B, makes a one electron (radical) pathway highly unlikely;³⁶ we therefore focused on the direct hydride transfer from the substrate $\text{C}\alpha\text{--H}$ moiety to the DAO cofactor, which is analogous to the mechanism proposed for the MAO-catalyzed oxidative deamination of amine substrates.^{36–41} We note that it has been recently shown, both experimentally and computationally, that C–H hydrogen bond donors directly transfer the hydride anion to the carbonyl oxygen of 2,3-dichloro-5,6-dicyano-1,4-benzoquinone, which is often used model quinone in mechanistic studies.^{42,43} Moreover, copper-promoted hydride transfer to a carbonyl group was previously reported as well.⁴⁴ Therefore, we modeled the reaction where $\text{C}\alpha\text{--H}$ hydride cleavage from the histamine substrate involves a direct transfer of the hydride anion (H^-) to the carbonyl O5-atom of the TPQ cofactor (Figure 2). QM calculations were

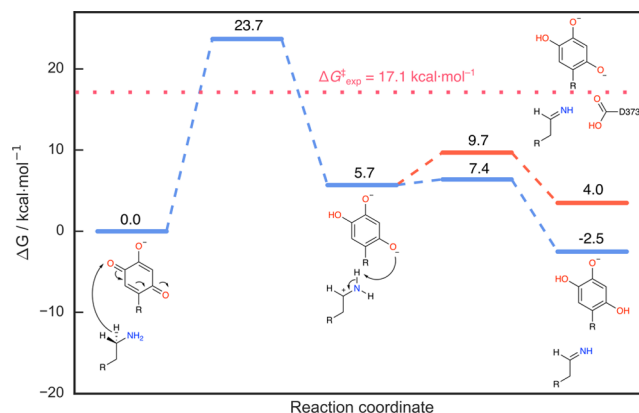
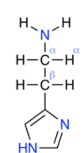
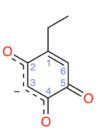


Figure 2. Free energy profile for the direct $\text{C}\alpha\text{--H}$ hydride transfer in *h*DAO-catalyzed deamination of histamine, obtained using a QM cluster model (blue). The feasible, but slightly less favorable, mechanistic alternative involving histamine deprotonation by the side chain of the active site D373 in the second step of the reductive half-reaction is shown in red. The experimental activation energy is displayed in pink. All energies are in $\text{kcal}\cdot\text{mol}^{-1}$. A simplified version of the cluster model used in the present work, showing only the main reacting atoms, is also presented for clarity.

performed using the same cluster model of the enzyme as described above. For the reaction coordinate, we selected the distance between the donor $\text{C}\alpha\text{--H}$ atom of the histamine and the carbonyl O5 atom of the TPQ cofactor. All calculations were performed at the (CPCM)/M11L/6-311++G(2df,2pd)-SDD/(CPCM)/M11L/6-31G(d)-SDD level of theory, as described in the Methodology section.

Table 1. Charge Distribution of the Reacting Atoms during the Rate-Limiting Hydride-Abstraction Step in hDAO-Catalyzed Histamine Oxidation^a

System	Specie	Isolated ^b	RS	TS	IS
	N (amino)	−0.97	−0.96	−0.80	−0.73
	α-H	0.22	0.22	0.43	0.52
	α-C	−0.23	−0.23	−0.13	0.28
	β-C	−0.52	−0.52	−0.52	−0.57
	total histamine	0.00	0.02	0.25	0.80
	C5	0.54	0.57	0.32	0.27
	O5	−0.60	−0.60	−0.70	−0.77
	C2	0.51	0.55	0.51	0.41
	O2	−0.70	−0.65	−0.72	−0.85
	total TPQ	−1.00	−1.02	−1.25	−1.40

^aPartial charges were obtained by NBO analysis⁴⁶ of the optimized geometries at the (CPCM)/M11L/6-31G(d)-SDD level of theory. ^b“Isolated” refers to the charges of the isolated fragments at infinite separation, and RS, TS, and IS indicate the corresponding reactant state, transition state, and intermediate state, respectively.

Figure 2 shows the relevant QM-optimized stationary points for the DAO catalyzed oxidative degradation of histamine. The relevant interaction distances are shown in Table S1, and the corresponding coordinates are provided in the Supporting Information. In the reactant state, the histamine is oriented toward the TPQ cofactor in a favorable conformation for the reaction to occur, forming hydrogen bonds between its amino group and the side-chain carboxylate of D373, as well between the histamine-ring imino nitrogen and the side-chain oxygen atom of Y459. The distances between the reacting atoms of histamine and TPQ at the reactant state, i.e., Cα–O5 and Hα–O5, are 3.2 and 2.6 Å, respectively. At the transition state, the hydrogen being transferred is asymmetrically located between the Cα-carbon and the O5-acceptor atom on the TPQ cofactor, with Cα–H and O5–H distances of 1.4 and 1.1 Å, respectively. We note here that the calculated activation free energy for this process is 23.7 kcal·mol^{−1} ($\nu_{\text{imag}} = 1012i \text{ cm}^{-1}$), which is significantly higher than the experimental value (17.1 kcal·mol^{−1},⁸ derived from the experimentally obtained k_{cat} of 139 min^{−1}, using the Eyring–Polanyi equation⁴⁵), and therefore, further EVB simulations^{20–22} were performed to probe this reaction, as described in the next section. We, however, note that the activation free energy of 23.7 kcal·mol^{−1} is comparable to the value of 24.4 kcal·mol^{−1} for the analogous reaction in MAO B that we previously obtained using the same QM-only cluster approach.³³

Natural bond orbital (NBO)⁴⁶ analysis of the QM optimized geometries demonstrates that this process is indeed associated with the transfer of a hydride anion, as can be seen from the calculated atomic charges (Table 1). In the reactant state, the sum of the partial charges on the atoms of histamine and the TPQ cofactor are 0.02 and −1.02, respectively. However, at the transition state, the partial charges change to 0.25 and −1.25, respectively, indicating a transfer of negative charge to the TPQ cofactor. Following the hydride abstraction, the system proceeds to the corresponding intermediates, characterized by the semireduced TPQ cofactor and the cationic substrate (Figures 1 and 2). The charge distribution further indicates that the formation of the new O5–H bond increases the total negative charge on the TPQ cofactor to −1.40, while simultaneously the total positive charge on the histamine

increases to 0.80. The following step in the amine oxidation involves deprotonation of the substrate amino group by the O2 atom of the TPQ cofactor (for a definition of the atom naming, see Table 1). This step is facilitated by the increase in the negative charge on the O2 atom of the TPQ cofactor during the hydride transfer reaction. This process is calculated to have a very low activation energy of 1.7 kcal·mol^{−1} ($\nu_{\text{imag}} = 1056i \text{ cm}^{-1}$) and is thus facile, making the initial hydride abstraction the rate-limiting step of the overall reaction. Finally, the overall reaction free energy (relative to the reactant state) is −2.5 kcal·mol^{−1}, resulting in a neutral trans-imine and fully reduced TPQ cofactor as the final products (Figure 2).

To explore the putative role of the active site residue D373 in deprotonating the cationic substrate during the second step of the reaction, as an alternative to the O2 atom of the TPQ cofactor, we also examined this pathway (Figure 2). Our calculations show that such a pathway is plausible, although the reaction proceeds through the transition state with a notably higher activation energy (4 kcal·mol^{−1} relative to the intermediate and 9.7 kcal·mol^{−1} relative to the reactant state) and with a slightly less stable product state ($\Delta G_0 = 4.0 \text{ kcal·mol}^{-1}$). However, both pathways are substantially lower in energy than the initial hydride transfer step and are therefore likely to be viable options to complete the reaction.

EVB Simulations. While our calculations using the QM cluster model strongly suggest that DAO utilizes a hydride transfer mechanism similar to that in MAO B, the calculated activation energy of 23.7 kcal·mol^{−1} is substantially higher than the experimental value of 17.1 kcal·mol^{−1}.⁸ This discrepancy could, in part, be due to either an incomplete electrostatic treatment in the continuum solvent model or due to insufficient conformational sampling. To address these issues, we complemented our QM cluster calculations with EVB^{20–22} simulations using the two-state model described in Figure S2.

A fundamental part of the EVB philosophy is the need for a well-defined reference state, which can be either the non-enzymatic reaction in vacuum or in solution or the WT enzyme against a series of mutants (see detailed discussion in, e.g., refs 21, 22). The reference state is then parameterized to reproduce either experimental data, where available, or higher-level QM calculations, where experimental data is lacking. The obtained

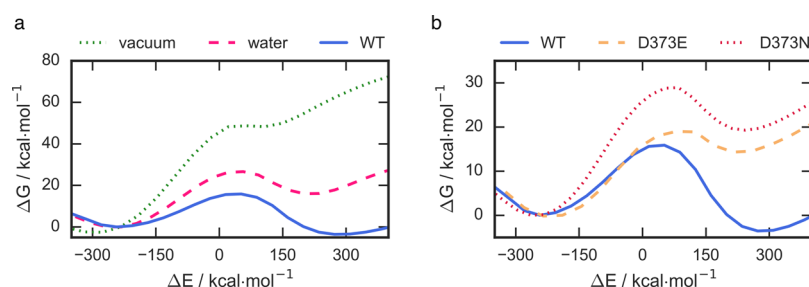


Figure 3. Averaged EVB free-energy profiles (over 10 independent trajectories) for the reaction catalyzed by DAO in (a) vacuum, aqueous solution, and the *h*DAO active site, and (b) WT *h*DAO and its D373E and D373N mutants. The generalized reaction coordinate (ΔE) is defined by the difference between the potential surfaces of the reactant and product states, as described in refs 21, 22.

parameters are then transferred to describe the same chemical reaction in different environments. Such an approach is feasible because of the demonstrated phase-independence of the EVB off-diagonal elements, as validated in ref 47. In the present case, due to the lack of experimental data to describe non-enzymatic histamine degradation in aqueous solution, it is necessary to fit the non-enzymatic reference state to energies obtained from higher-level QM calculations. For simplicity, we have performed our reference calculations in vacuum to avoid artifacts introduced by using continuum rather than explicit solvation. We then performed EVB simulations in vacuum, as described in the Methodology section, fitting to the quantum chemical calculations, and then using the same parameters to study the reaction in solution and the DAO active site, as in previous work.^{38,41} The vacuum energetics of the reaction were calculated at the M11L/6-31G(d) level of theory, with zero-point energies and entropies calculated from the vibrational frequencies at the same level of theory as the geometry optimizations. The model for the direct hydride transfer reaction consisted of neutral histamine and TPQ cofactor with a deprotonated hydroxyl group. The obtained transition state was verified by frequency analysis ($\nu_{\text{imag}} = 745i \text{ cm}^{-1}$), as well as by following the intrinsic reaction coordinate in the reactant and product directions,⁴⁸ which yielded an activation free energy, ΔG^\ddagger , of 51.5 kcal·mol⁻¹, and a reaction free energy, ΔG_0 , of 50.8 kcal·mol⁻¹. These extremely large values are consistent with the expectation that the investigated hydride transfer would be extremely unfavorable in the gas phase.

The EVB free energies, obtained using the calibration parameters shown in Table S2, are given in Figure 3a. As our QM cluster calculations indicated that the hydride transfer is the rate-limiting step of the overall process, we have focused only on this step in our EVB calculations. From this data, it can be seen that, as expected, the inclusion of solvent effects already substantially reduces the hydride transfer barrier even for the non-enzymatic reaction. The barrier is further reduced in the *h*DAO active site, yielding a calculated activation free energy of 14.8 kcal·mol⁻¹. Previous studies have shown that protonated histamine is likely bound to the active site; however, deprotonated (neutral) histamine is essential for the reaction to take place. Thus, an intraenzymatic deprotonation of histamine must occur within the enzyme active site, the cost of which would be expected to be 2.7 kcal·mol⁻¹ at physiological pH (assuming a pK_a of 9.4 for histamine and using the relationship $\Delta G_{\text{PT}} = 2.303RT(pK_a(\text{donor}) - \text{pH})$). The cost of this deprotonation, which approximately equals the difference between the calculated free energy of activation of 14.8 kcal·mol⁻¹ and the experimental value of 17.1 kcal·mol⁻¹ (derived from $k_{\text{cat}} = 139 \text{ min}^{-1}$),⁸ needs to be added to the

calculated value to account for the initial histamine deprotonation. This yields an overall calculated free energy of 17.5 kcal·mol⁻¹, in excellent agreement with the experimental value, thus giving credence to our proposed mechanism (Table 2).

Table 2. Catalytic Rate Constants (k_{cat}), Experimental and Calculated (EVB) Free Energies of Activation (ΔG^\ddagger) and Reaction (ΔG_0) for Histamine Oxidation in Vacuum, Aqueous Solution, and by the Selected DAO Variants^a

	k_{cat}	$\Delta G_{\text{exp}}^\ddagger$	$\Delta G_{\text{calc}}^\ddagger$	$\Delta \Delta G^\ddagger$	$\Delta G_{0,\text{calc}}$
vacuum	^b		51.5 ± 0.3		50.8 ± 0.2
water	^b		26.6 ± 0.2		15.6 ± 0.3
<i>h</i> DAO	139 ^c	17.1	14.8 ± 1.0	0	-2.9 ± 1.5
D373E <i>h</i> DAO	^b		19.4 ± 0.1	4.6	14.1 ± 0.9
D373N <i>h</i> DAO	^b		29.1 ± 0.3	14.3	19.9 ± 0.3
<i>ec</i> AO	2073 ^d	15.4	^e	0	
D383E <i>ec</i> AO	0.084 ^d	21.5	^e	6.1	

^aAll k_{cat} values are shown in min⁻¹ and ΔG values are shown in kcal·mol⁻¹. $\Delta G_{\text{exp}}^\ddagger$ values were computed from k_{cat} using the Eyring–Polanyi equation. Calculated free energies represent average values and standard deviations over 10 independent EVB runs, performed as described in the Methodology section. ^bExperimental data not available. ^cExperimental data from ref 8. ^dExperimental data from ref 14, computed from the specific activity given in $\mu\text{mol}\cdot\text{mg}^{-1}\cdot\text{min}^{-1}$, with molecular weight taken from *ec*AO (PDB ID: 1SPU). ^eVariant not simulated.

Finally, we note that our EVB calculations predict an activation free energy of 26.6 kcal·mol⁻¹ for the non-enzymatic reaction in aqueous solution, leading to a barrier reduction of 11.8 kcal·mol⁻¹ upon moving to the enzyme active site. This would correspond to a tremendous rate acceleration of 10⁹-fold compared to the non-enzymatic reaction. This substantial rate enhancement is comparable in magnitude to the similarly large rate enhancement observed computationally in MAO B-catalyzed dopamine oxidation, which has been demonstrated to operate through the same direct hydride transfer mechanism.³⁸ The hydride transfer is also predicted to be thermodynamically favorable, with a calculated reaction free energy, ΔG_0 , of -2.9 kcal·mol⁻¹.

Roles of D373 and the Metal Cofactor. Following from our modeling of the WT enzyme, we have also investigated the role of D373 in the catalytic mechanism by mutating this residue both to glutamine and the isostructural, but chemically distinct, asparagine (Figure 4). It was experimentally shown that the D373E mutation leads to low but still detectable activity, whereas the corresponding mutation to asparagine completely abolishes the catalytic activity (Table 2).¹⁴ On the

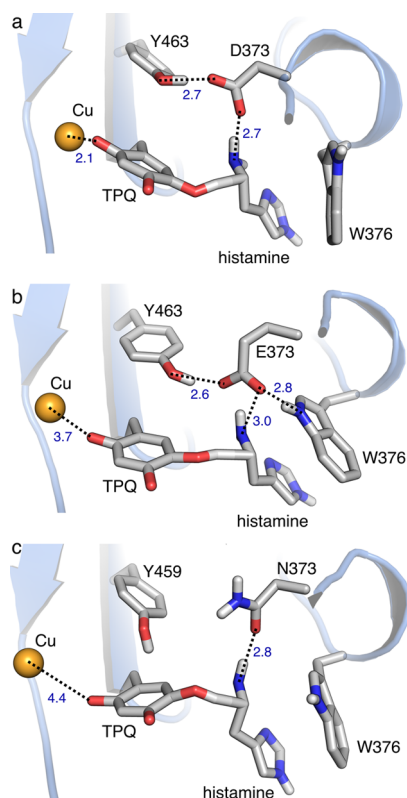


Figure 4. Representative EVB transition state structures for the reactions catalyzed by (a) WT *hDAO* and its (b) D373E and (c) D373N mutants in complex with histamine. The average distances between the active site residues, computed over the TS trajectory, are shown in Å, and the complete statistics is provided in Table S3.

basis of this, it has been proposed that D373 acts as the catalytic base by abstracting proton from the substrate–Schiff base complex to produce the product–Schiff base complex (Scheme 3, :B[−]). However, we demonstrate here (Table 2) that we obtain good agreement with experiment when modeling this reaction as proceeding through a direct hydride transfer mechanism. Specifically, as can be seen from the obtained EVB energetics, the calculated activation free energy for the rate-limiting step of direct hydride transfer in the D373N *hDAO* variant is 29.1 kcal·mol^{−1}, which is a loss in activity of approximately 10 orders of magnitude compared to that calculated for the WT enzyme (with $\Delta G_{\text{calc}}^{\ddagger} = 14.8$ kcal·mol^{−1}). Also, there is an extremely high thermodynamic barrier to this process, as reflected in the reaction free energy of 19.9 kcal·mol^{−1}. Therefore, our calculations predict a complete loss of activity for this variant, based on the direct hydride transfer mechanism. Following from this, in the case of the D373E variant, we calculate an activation free energy of 19.4 kcal·mol^{−1}, in reasonable agreement with the experimental value of 21.5 kcal·mol^{−1} for *ecAO*.¹⁴ We also note that in the case of *ecAO*, this mutation increases the activation free energy by 6.1 kcal·mol^{−1}. While we do not have the corresponding experimental value for the *hDAO* mutants, our calculated $\Delta\Delta G_{\text{calc}}^{\ddagger}$ of 4.6 kcal·mol^{−1} for mutant versus WT *hDAO* is in good agreement with the observations from *E. coli* (where $\Delta\Delta G_{\text{exp}}^{\ddagger}$ is 6.1 kcal·mol^{−1}). Here, we take into account that, as shown in Table 2, WT *hDAO* is less active than the corresponding enzyme from *E. coli*.

From a structural perspective, our EVB simulations show that, in the calculated transition states (Figure 4a), D373 forms

hydrogen bonds with the amino group of histamine (average distance 2.7 ± 0.1 Å and average angle $165.4 \pm 7.9^\circ$) and with the side chain of Y463 (2.7 ± 0.1 Å). In the transition state of the D373E mutant, however, E373 forms hydrogen bonds primarily with W376 (2.8 ± 0.2 Å) and Y463 (2.6 ± 0.1 Å), thus bridging the two residues and not being engaged in hydrogen bonding with amino group of histamine (3.0 ± 0.2 Å and $142.7 \pm 13.8^\circ$), which implies that this hydrogen bond is lost at the transition state. At the same time, the average distance between the cofactor TPQ:O2 and Cu²⁺ cation is 2.10 ± 0.03 Å for WT *DAO* in contrast to 3.7 ± 0.2 Å for D373E. This distance further increases to 4.4 ± 0.1 Å for the D373N mutant (Figure 4). The electrostatic contributions of the most significant residues (Figure 5) show that the protein residue at

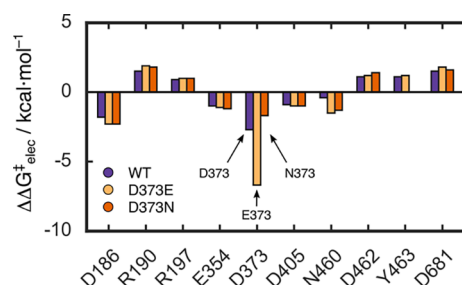


Figure 5. Electrostatic contributions of the most significant residues (with a contribution >1 kcal·mol^{−1}) to the calculated activation free energies ($\Delta\Delta G_{\text{elec,RS} \rightarrow \text{TS}}^{\ddagger}$) of the *hDAO*-catalyzed direct hydride transfer reaction. The depicted values were obtained by applying the linear response approximation to the calculated EVB trajectories and scaled by assuming an active site dielectric constant of 4, as in our previous work (ref 49).

position 373 (i.e., D in the wild type, E or N in mutants) affects catalysis the most (while some other residues also make contributions, as annotated in this figure, the contributions are similar between the different enzyme variants, and mostly cancel each out). Thus, the difference in the free energy of activation between the WT and D373E or D373N mutant enzyme may be explained by a combination of the loss of stabilizing interactions from the catalytic Cu²⁺ cation, together with (in the case of the N373 variant) a slight loss of stabilizing interaction from D373, which in turn leads to the loss of activity.

CONCLUSIONS

In this work, we combined QM cluster calculations and EVB simulations to elucidate the catalytic mechanism of the *DAO* catalyzed oxidative deamination of histamine. Our results indicate that direct hydride transfer from the substrate C α –H moiety to the OS atom of TPQ cofactor is the rate-limiting step of the reductive half-reaction, which is in line with the experimentally confirmed rate-limiting step. EVB simulations of the hydride transfer reaction catalyzed by WT *DAO* predict an almost 9 orders of magnitude rate enhancement in comparison to the corresponding non-enzymatic reaction in aqueous solution. The same rate enhancement was observed for the equivalent reaction catalyzed by the MAO B enzyme on monoamines.³⁸ Moreover, we have also shown that while D373 is indeed essential for *DAO* catalysis, its role is not proton abstraction during the catalytic cycle, as previously proposed.^{12–14} Namely, the average hydrogen bond distances at the transition state combined with the electrostatic contribu-

tions of the most significant residues (in terms of energetic contributions) to the calculated activation free energies showed that proximity of the Cu^{2+} cation, together with the residue D373, affect catalysis the most, with the loss of key interactions with these moieties leading to the observed loss of activities in the D373E and D373N variants. In conjunction with our previous work,⁴⁰ the results presented here suggest that the in vivo degradation of histamine to yield an aldehyde always occurs via the same catalytic mechanism, namely direct hydride transfer from histamine and *N*-methylhistamine to the corresponding cofactor (TPQ or FAD, respectively), regardless of the histamine catabolic pathway. A detailed understanding of the mechanism of histamine-degrading enzymes is important for the design of therapeutics for the treatment of histamine intolerance, bearing in mind that no medication to date is able to increase DAO activity and therefore keep the level of histamine degradation in balance. Insufficient histamine degradation by DAO however may also disrupt the other histamine-degrading pathway operating through HNMT and MAO B, resulting in the collapse of histamine clearance.^{50,51} Therefore, the catalytic mechanism of the degradation of this possibly harmful compound is important for the successful development of drugs that could supplement impaired histamine-degradation pathways.

METHODOLOGY

QM Calculations. The cluster model of the DAO active site used in this work consisted of the substrate histamine, the Cu^{2+} cation, the TPQ cofactor, and the active site residues D373, Y371, W376, Y459, H510, H512, and H675, as shown in Figure 1. Geometries for all key stationary points were optimized using the M11L functional⁵² at the M11L/6-31G(d) level of theory, with the thermal Gibbs free energy corrections extracted from frequency calculations at the same level of theory without scaling factors applied. A further single point calculation was performed with the larger 6-311++G(2df,2pd) basis set to refine the electronic energies. The results of these calculations are shown in Figure 2 and Table S4.

System Setup for the EVB Simulations. To calibrate our EVB simulations of the enzyme catalyzed reactions, we performed corresponding simulation of the non-enzymatic reaction in vacuum. The EVB gas-phase shift and coupling parameters (α_2^0 and H_{12} , Table S2) were obtained by fitting these simulations to ΔG^\ddagger and ΔG_0 obtained from QM calculations in vacuum at the M11L/6-31G(d) level of theory and then using the same parameter set for the reactions in aqueous solution and in the enzyme active site. All QM calculations are performed using the Gaussian 09 package.⁵³

The starting points for our EVB simulations of DAO were the coordinates of DAO in complex with the inhibitor aminoguanidine (PDB ID: 3MPH).⁵⁴ The D373E and D373N mutants of DAO were generated using the Dunbrack backbone-dependent rotamer library,⁵⁵ as implemented in Chimera.⁵⁶ The position of the inhibitor in this structure served as a reference point for initial manual positioning of the substrate (i.e., histamine) into the hDAO active site. Short MD simulations of 5 ns were then performed to obtain equilibrated and optimized structures, which served as a starting point for the subsequent protein parameterization. The protein model included one subunit of hDAO enclosed in a simulation sphere, with a 30 Å radius, centered at the reactive C α of the substrate. All protein atoms outside this sphere were kept restrained to their starting positions by applying a 200 kcal·mol⁻¹·Å⁻²

harmonic restraint. All ionized residues in simulations are listed in Table S5. Other ionizable residues outside this region were kept in their neutral state. All simulations were performed using the OPLS-AA force field,^{57,58} and the copper ion in this enzyme was reparametrized to reproduce the correct tetrahedral coordination, based on the previously published copper dummy model by Liao et al.⁵⁹ This model has been successful in reproducing the Jahn–Teller effect seen in divalent copper and was deemed an excellent starting point for the reparametrization.

All molecular dynamics and EVB simulations in this work were performed using the Q (v5.10) simulation package.⁶⁰ The resulting structure of DAO in complex with histamine was equilibrated and gradually heated to 300 K over a short 25 ps simulation. The system was further equilibrated at 300 K, performing 10 ns of MD simulation starting at the transition state, for each reaction. An initial 200 kcal·mol⁻¹·Å⁻² harmonic restraint was applied on all heavy atoms in the simulation sphere to remove bad contacts. This was gradually reduced during the initial heating phase, while only a 0.5 kcal·mol⁻¹·Å⁻² restraint was left on the reacting atoms of the substrate histamine and TPQ cofactor. All solvent hydrogen atoms were constrained by the SHAKE algorithm,⁶¹ and system temperatures were regulated using the Berendsen thermostat⁶² with a 100 fs bath relaxation time. For the calculation of all nonbonded interactions, a cut-off value of 10 Å was used, with the exception of those involving reacting atoms for which a 99 Å cut-off (i.e., no cut-off) was used. The endpoint structure of the equilibration run was used as a starting point for the subsequent EVB simulations. The equilibrated structure was subjected to 10 parallel FEP runs by randomizing the atomic velocities to perform independent EVB calculations and ensure reliable sampling. The mapping procedure was performed in 51 mapping frames of 100 ps each, yielding a total simulation time of 5.1 ns per replica.

Substrate and Cofactor Parameterization. The program Q⁶⁰ used for the EVB simulations, and GROMACS,⁶³ which was employed in the original Cu-model paper, use different force field descriptions and the former does not apply particle mesh Ewald summation for the long-range electrostatic interactions. Therefore, the published Cu parameters were further validated and optimized to allow a better fit with the previous experimental data.⁶⁴ For the new parameters, both the repulsive and attractive parts of the center particle of the ion model were optimized in respect to the resulting hydration free energies and ion–water radial distribution functions. It was also necessary to reduce the repulsive force on the non-interacting dummy particles from the 0.03 kcal·mol⁻¹·Å⁻⁶, used in the previous dummy model paper,⁶⁵ to 0.01 kcal·mol⁻¹·Å⁻⁶, or the reproduction of the Jahn–Teller distortions was not possible. This setup is in line with the results obtained in the original article with GROMACS, where no force at all was applied to the dummy particles. This approach was not chosen to avoid singularities when calculating the forces in Q.

The parameterization was performed using the TIP3P water model as implemented in Q, with the dummy model being solvated in an 18 Å water sphere subjected to the spherical boundary conditions, according to the surface-constrained all-atom solvent model.⁶⁶ Hydrogen atoms were subjected to the SHAKE algorithm, with long-range interactions beyond a cut-off of 10 Å being treated using the LRF approach.⁶⁷ The metal dummy was kept in the simulation sphere by applying a weak position restraint of 0.5 kcal·mol⁻¹·Å⁻². After relaxing the

system by gradually increasing temperature over the course of 60 ps, the final coordinates were used to start five independent calculations of the solvation free energy, using 51 umbrella-sampling windows of 100 ps simulation time each (5.1 ns simulation time per trajectory). The analysis of the free energies was performed using the Qfep tool of the Q program suite. The radial distribution function was calculated, from three 1 ns-long independent MD simulations, using VMD (1.9.1),⁶⁸ employing a bin size of 0.01 and a cut-off of 10 Å (Figure S3).

The parameters for nonstandard protein residues (substrate and cofactor) were obtained using the ffd server as implemented in Schrödinger's MacroModel suite⁶⁹ allowing for the construction of the relevant EVB force fields to correctly describe the reactant and product states of the hDAO-catalyzed reaction (Tables S6–S10). For both states, atomic charges were determined by fitting to the electrostatic potentials computed by the QM calculations at the HF/6-31G(d) level of theory according to the RESP scheme, as implemented in AmberTools15.⁷⁰

■ ASSOCIATED CONTENT

■ Supporting Information

The Supporting Information is available free of charge on the ACS Publications website at DOI: 10.1021/acsomega.8b00346.

Additional computational data and all parameters necessary to reproduce our EVB simulations (PDF)

■ AUTHOR INFORMATION

Corresponding Authors

*E-mail: robert.vianello@irb.hr (R.V.).

*E-mail: kamerlin@icm.uu.se (S.C.L.K.).

ORCID

Aleksandra Maršavelski: 0000-0003-1139-7173

Dušan Petrović: 0000-0002-1834-7358

Robert Vianello: 0000-0003-1779-4524

Shina Caroline Lynn Kamerlin: 0000-0002-3190-1173

Notes

The authors declare no competing financial interest.

■ ACKNOWLEDGMENTS

A.M. thanks the Federation of European Biochemical Societies for a Short-Term Fellowship which allowed her to visit the Kamerlin lab in Uppsala, Sweden, where the EVB simulations were performed. A.M. also thanks the Croatian Science Foundation for a PhD fellowship through the Career Development Project for Young Researchers (contract number I-3376-2014). R.V. gratefully acknowledges the Croatian Science Foundation for a financial support through the project IP-2014-09-3386. S.C.L.K. thanks the Swedish Research Council (VR, grant 2015-04928) for funding and support, as well as the Swedish National Infrastructure for Computing, SNIC, for the generous allocation of supercomputing time (SNIC 2016/34-27 and 2017/12-11).

■ REFERENCES

- (1) McIntire, W. S.; Hartmann, C. Copper-Containing Amine Oxidases. In *Principles and Applications of Quinoproteins*; Davison, V. L., Ed.; Marcel Dekker Inc.: New York, 1993; pp 97–171.
- (2) Klinman, J. P.; Mu, D. Quinooenzymes in Biology. *Annu. Rev. Biochem.* **1994**, *63*, 299–344.

- (3) Knowles, P. F.; Dooley, D. M. Amine Oxidase. In *Metal Ions in Biological Systems*; Sigel, H., Sigel, A., Eds.; Marcel Dekker: New York, 1994; pp 361–403.

- (4) Maintz, L.; Novak, N. Histamine and Histamine Intolerance. *Am. J. Clin. Nutr.* **2007**, *85*, 1185–1196.

- (5) Edmondson, D. E.; Bhattacharyya, A. K.; Walker, M. C. Spectral and Kinetic Studies of Imine Product Formation in the Oxidation of P-(N,N-Dimethylamino)benzylamine Analogues by Monoamine Oxidase B. *Biochemistry* **1993**, *32*, 5196–5202.

- (6) Gaweska, H.; Fitzpatrick, P. F. Structures and Mechanism of the Monoamine Oxidase Family. *Biomol. Concepts* **2011**, *2*, 365–377.

- (7) Hough, L. B.; Leurs, R. Histamine. In *Basic Neurochemistry: Molecular, Cellular, and Medical Aspects*, 6th ed.; Siegel, G. J., Albers, R. W., Brady, S. T., Price, D. L., Eds.; Academic Press: New York, 2006; pp 249–262.

- (8) Elmore, B. O.; Bollinger, J. A.; Dooley, D. M. Human Kidney Diamine Oxidase: Heterologous Expression, Purification, and Characterization. *J. Biol. Inorg. Chem.* **2002**, *7*, S65–S79.

- (9) Schayer, R. W.; Smiley, R. L.; Kennedy, J. Diamine Oxidase and Cadaverine Metabolism. *J. Biol. Chem.* **1954**, *206*, 461–464.

- (10) Karlson, P. Transamination. In *Introduction to Modern Biochemistry*, 4th ed.; Karlson, P., Ed.; Academic Press: New York, 1975; p 173.

- (11) Bardsley, W. G.; James, M.; Crabbe, C.; Shindler, J. S. Kinetics of the Diamine Oxidase Reaction. *Biochem. J.* **1973**, *131*, 459–469.

- (12) Mure, M.; Klinman, J. P. Model Studies of Topaquinone-Dependent Amine Oxidases. 2. Characterization of Reaction Intermediates and Mechanism. *J. Am. Chem. Soc.* **1995**, *117*, 8707–8718.

- (13) Wilmot, C. M.; Murray, J. M.; Alton, G.; Parsons, M. R.; Convery, M. A.; Blakeley, V.; Corner, A. S.; Palcic, M. M.; Knowles, P. F.; McPherson, M. J.; Phillips, S. E. V. Catalytic Mechanism of the Quinooenzyme Amine Oxidase from *Escherichia coli*: Exploring the Reductive Half-Reaction. *Biochemistry* **1997**, *36*, 1608–1620.

- (14) Murray, J. M.; Saysell, C. G.; Wilmot, C. M.; Tambyrajah, W. S.; Jaeger, J.; Knowles, P. F.; Phillips, S. E. V.; McPherson, M. J. The Active Site Base Controls Cofactor Reactivity in *Escherichia coli* Amine Oxidase: X-Ray Crystallographic Studies with Mutational Variants. *Biochemistry* **1999**, *38*, 8217–8227.

- (15) Klement, V. J.; Wilmot, C. M. The Role of Protein Crystallography in Defining the Mechanisms of Biogenesis and Catalysis in Copper Amine Oxidase. *Int. J. Mol. Sci.* **2012**, *13*, 5375–5405.

- (16) Kataoka, M.; Oya, H.; Tominaga, A.; Otsu, M.; Okajima, T.; Tanizawa, K.; Yamaguchi, H. Detection of the Reaction Intermediates Catalyzed by a Copper Amine Oxidase. *J. Synchrotron Radiat.* **2011**, *18*, 58–61.

- (17) Padiglia, A.; Medda, R.; Lorrai, A.; Congiu, D.; Pedersen, J. Z.; Floris, G. Oxidation of Kynuramine by Lentil Seedling Copper Amine Oxidase: Demonstration of a Single Turnover Mechanism in the Apoenzyme. *Phytochem. Anal.* **1998**, *9*, 223–226.

- (18) Mura, A.; Padiglia, A.; Medda, R.; Pintus, F.; Agrò, A. F.; Floris, G. Properties of Copper-Free Pig Kidney Amine Oxidase: Role of Topa Quinone. *FEBS Lett.* **2006**, *580*, 4317–4324.

- (19) Himo, F. Recent Trends in Quantum Chemical Modeling of Enzymatic Reactions. *J. Am. Chem. Soc.* **2017**, *139*, 6780–6786.

- (20) Warshel, A.; Weiss, R. M. An Empirical Valence Bond Approach for Comparing Reactions in Solutions and in Enzymes. *J. Am. Chem. Soc.* **1980**, *102*, 6218–6226.

- (21) Warshel, A. Simulating Metalloenzymes. *Computer Modeling of Chemical Reactions in Enzymes and Solutions*; John Wiley & Sons, Inc.: Chichester, 1997; pp 189–208.

- (22) Shurki, A.; Derat, E.; Barrozo, A.; Kamerlin, S. C. L. How Valence Bond Theory Can Help You Understand Your (Bio)chemical Reaction. *Chem. Soc. Rev.* **2015**, *44*, 1037–1052.

- (23) Saysell, C. G.; Tambyrajah, W. S.; Murray, J. M.; Wilmot, C. M.; Phillips, S. E. V.; McPherson, M. J.; Knowles, P. F. Probing the Catalytic Mechanism of *Escherichia coli* Amine Oxidase Using

Mutational Variants and a Reversible Inhibitor as a Substrate Analogue. *Biochem. J.* **2002**, 365, 809–816.

(24) Maintz, L.; Bieber, T.; Novak, N. Histamine Intolerance in Clinical Practice. *Dtsch. Arzteblatt* **2006**, 103, A3477–3483.

(25) Mure, M.; Brown, D. E.; Saysell, C.; Rogers, M. S.; Wilmot, C. M.; Kurtis, C. R.; McPherson, M. J.; Phillips, S. E. V.; Knowles, P. F.; Dooley, D. M. Role of the Interactions between the Active Site Base and the Substrate Schiff Base in Amine Oxidase Catalysis. Evidence from Structural and Spectroscopic Studies of the 2-Hydrazinopyridine Adduct of *Escherichia coli* Amine Oxidase. *Biochemistry* **2005**, 44, 1568–1582.

(26) Siegbahn, P. E. M.; Himo, F. The Quantum Chemical Cluster Approach for Modeling Enzyme Reactions. *Wiley Interdiscip. Rev. Comput. Mol. Sci.* **2011**, 1, 323–336.

(27) Tantillo, D. J.; Chen, J.; Houk, K. N. Theozymes and Compuzymes: Theoretical Models for Biological Catalysis. *Curr. Opin. Chem. Biol.* **1998**, 2, 743–750.

(28) Tantillo, D. J.; Houk, K. N. Theozymes and Catalyst Design. *Stimulating Concepts in Chemistry*; Wiley, 2005; pp 79–88.

(29) Cossi, M.; Rega, N.; Scalmani, G.; Barone, V. Energies, Structures, and Electronic Properties of Molecules in Solution with the C-PCM Solvation Model. *J. Comput. Chem.* **2003**, 24, 669–681.

(30) Bardsley, W. G.; Ashford, J. S.; Hill, C. M. Synthesis and Oxidation of Aminoalkyl-Onium Compounds by Pig Kidney Diamine Oxidase. *Biochem. J.* **1971**, 122, 557–567.

(31) Hartmann, C.; Klinman, J. P. Structure-Function Studies of Substrate Oxidation by Bovine Serum Amine Oxidase: Relationship to Cofactor Structure and Mechanism. *Biochemistry* **1991**, 30, 4605–4611.

(32) Farnum, M.; Palcic, M.; Klinman, J. P. pH Dependence of Deuterium Isotope Effects and Tritium Exchange in the Bovine Plasma Amine Oxidase Reaction: A Role for Single-Base Catalysis in Amine Oxidation and Imine Exchange. *Biochemistry* **1986**, 25, 1898–1904.

(33) Borštnar, R.; Repič, M.; Kamerlin, S. C. L.; Vianello, R.; Mavri, J. Computational Study of the pK(a) Values of Potential Catalytic Residues in the Active Site of Monoamine Oxidase B. *J. Chem. Theory Comput.* **2012**, 8, 3864–3870.

(34) Mure, M.; Klinman, J. P. Synthesis and Spectroscopic Characterization of Model Compounds for the Active Site Cofactor in Copper Amine Oxidases. *J. Am. Chem. Soc.* **1993**, 115, 7117–7127.

(35) Moenne-Loccoz, P.; Nakamura, N.; Steinebach, V.; Duine, J. A.; Mure, M.; Klinman, J. P.; Sanders-Loehr, J. Characterization of the Topa Quinone Cofactor in Amine Oxidase from *Escherichia coli* by Resonance Raman Spectroscopy. *Biochemistry* **1995**, 34, 7020–7026.

(36) Vianello, R.; Repič, M.; Mavri, J. How Are Biogenic Amines Metabolized by Monoamine Oxidases? *Eur. J. Org. Chem.* **2012**, 7057–7065.

(37) Vianello, R.; Domene, C.; Mavri, J. The Use of Multiscale Molecular Simulations in Understanding a Relationship between the Structure and Function of Biological Systems of the Brain: The Application to Monoamine Oxidase Enzymes. *Front. Neurosci.* **2016**, 10, 327.

(38) Repič, M.; Vianello, R.; Purg, M.; Duarte, F.; Bauer, P.; Kamerlin, S. C. L.; Mavri, J. Empirical Valence Bond Simulations of the Hydride Transfer Step in the Monoamine Oxidase B Catalyzed Metabolism of Dopamine. *Proteins: Struct., Funct., Bioinf.* **2014**, 82, 3347–3355.

(39) Oanca, G.; Purg, M.; Mavri, J.; Shih, J. C.; Stare, J. Insights into Enzyme Point Mutation Effect by Molecular Simulation: Phenylethylamine Oxidation Catalyzed by Monoamine Oxidase A. *Phys. Chem. Chem. Phys.* **2016**, 18, 13346–13356.

(40) Maršavelski, A.; Vianello, R. What a Difference a Methyl Group Makes: The Selectivity of Monoamine Oxidase B Towards Histamine and N-Methylhistamine. *Chem.—Eur. J.* **2017**, 23, 2915–2925.

(41) Poberžnik, M.; Purg, M.; Repič, M.; Mavri, J.; Vianello, R. Empirical Valence Bond Simulations of the Hydride-Transfer Step in the Monoamine Oxidase A Catalyzed Metabolism of Noradrenaline. *J. Phys. Chem. B* **2016**, 120, 11419–11427.

(42) Guo, X.; Zipse, H.; Mayr, H. Mechanisms of Hydride Abstractions by Quinones. *J. Am. Chem. Soc.* **2014**, 136, 13863–13873.

(43) Yamabe, S.; Yamazaki, S.; Sakaki, S. A DFT Study of Hydride Transfers to the Carbonyl Oxygen of DDQ. *Int. J. Quantum Chem.* **2015**, 115, 1533–1542.

(44) Tsuda, T.; Habu, H.; Saegusa, T. Effect of Ligands on Copper-Promoted Hydride Transfer to Carbonyl Group. *J. Chem. Soc., Chem. Commun.* **1974**, 620.

(45) Evans, M. G.; Polanyi, M. Some Applications of the Transition State Method to the Calculation of Reaction Velocities, Especially in Solution. *Trans. Faraday Soc.* **1935**, 31, 875–894.

(46) Glendenning, E. D.; Landis, C. R.; Weinhold, F. Natural Bond Orbital Methods. *Wiley Interdiscip. Rev. Comput. Mol. Sci.* **2012**, 2, 1–42.

(47) Hong, G.; Rosta, E.; Warshel, A. Using the Constrained DFT Approach in Generating Diabatic Surfaces and Off Diagonal Empirical Valence Bond Terms for Modeling Reactions in Condensed Phases. *J. Phys. Chem. B* **2006**, 110, 19570–19574.

(48) Fukui, K. The Path of Chemical Reactions - the IRC Approach. *Acc. Chem. Res.* **1981**, 14, 363–368.

(49) Kulkarni, Y. S.; Liao, Q.; Petrović, D.; Krüger, D. M.; Strodel, B.; Amyes, T. L.; Richard, J. P.; Kamerlin, S. C. L. Enzyme Architecture: Modeling the Operation of a Hydrophobic Clamp in Catalysis by Triosephosphate Isomerase. *J. Am. Chem. Soc.* **2017**, 139, 10514–10525.

(50) Sattler, J.; Häfner, D.; Klotter, H.-J.; Lorenz, W.; Wagner, P. K. Food-Induced Histaminosis as an Epidemiological Problem: Plasma Histamine Elevation and Haemodynamic Alterations after Oral Histamine Administration and Blockade of Diamine Oxidase (DAO). *Agents Actions* **1988**, 23, 361–365.

(51) Sattler, J.; Lorenz, W.; Kubo, K.; Schmal, A.; Sauer, S.; Lüben, L. Food-Induced Histaminosis under Diamine Oxidase (DAO) Blockade in Pigs: Further Evidence of the Key Role of Elevated Plasma Histamine Levels as Demonstrated by Successful Prophylaxis with Antihistamines. *Agents Actions* **1989**, 27, 212–214.

(52) Peverati, R.; Truhlar, D. G. M11-L: A Local Density Functional That Provides Improved Accuracy for Electronic Structure Calculations in Chemistry and Physics. *J. Phys. Chem. Lett.* **2012**, 3, 117–124.

(53) Frisch, M. J.; Trucks, G. W.; Schlegel, H. B.; Scuseria, G. E.; Robb, M. A.; Cheeseman, J. R.; Scalmani, G.; Barone, V.; Mennucci, B.; Petersson, G. A.; Nakatsuji, H.; Caricato, M.; Li, X.; Hratchian, H. P.; Izmaylov, A. F.; Bloino, J.; Zheng, G.; Sonnenberg, J. L.; Hada, M.; Ehara, M.; Toyota, K.; Fukuda, R.; Hasegawa, J.; Ishida, M.; Nakajima, T.; Honda, Y.; Kitao, O.; Nakai, H.; Vreven, T.; Montgomery, J. A., Jr.; Peralta, J. E.; Ogliaro, F.; Bearpark, M.; Heyd, J. J.; Brothers, E.; Kudin, K. N.; Staroverov, V. N.; Kobayashi, R.; Normand, J.; Raghavachari, K.; Rendell, A.; Burant, J. C.; Iyengar, S. S.; Tomasi, J.; Cossi, M.; Rega, N.; Millam, J. M.; Klene, M.; Knox, J. E.; Cross, J. B.; Bakken, V.; Adamo, C.; Jaramillo, J.; Gomperts, R.; Stratmann, R. E.; Yazyev, O.; Austin, A. J.; Cammi, R.; Pomelli, C.; Ochterski, J. W.; Martin, R. L.; Morokuma, K.; Zakrzewski, V. G.; Voth, G. A.; Salvador, P.; Dannenberg, J. J.; Dapprich, S.; Daniels, A. D.; Farkas, Ö.; Foresman, J. B.; Ortiz, J. V.; Cioslowski, J.; Fox, D. J. *Gaussian 09*. Revision D.01; Gaussian Inc.: Wallingford CT, 2010.

(54) McGrath, A. P.; Caradoc-Davies, T.; Collyer, C. A.; Guss, J. M. Correlation of Active Site Metal Content in Human Diamine Oxidase with Trihydroxyphenylalanine Quinone Cofactor Biogenesis. *Biochemistry* **2010**, 49, 8316–8324.

(55) Dunbrack, R. L. Rotamer Libraries in the 21st Century. *Curr. Opin. Struct. Biol.* **2002**, 12, 431–440.

(56) Pettersen, E. F.; Goddard, T. D.; Huang, C. C.; Couch, G. S.; Greenblatt, D. M.; Meng, E. C.; Ferrin, T. E. UCSF Chimera - A Visualization System for Exploratory Research and Analysis. *J. Comput. Chem.* **2004**, 25, 1605–1612.

(57) Kaminski, G. A.; Friesner, R. A.; Tirado-Rives, J.; Jorgensen, W. L. Evaluation and Reparametrization of the OPLS-AA Force Field for Proteins via Comparison with Accurate Quantum Chemical Calculations on Peptides. *J. Phys. Chem. B* **2001**, 105, 6474–6487.

- (58) Robertson, M. J.; Tirado-Rives, J.; Jorgensen, W. L. Improved Peptide and Protein Torsional Energetics with the OPLS-AA Force Field. *J. Chem. Theory Comput.* **2015**, *11*, 3499–3509.
- (59) Liao, Q.; Kamerlin, S. C. L.; Strodel, B. Development and Application of a Nonbonded Cu^{2+} Model That Includes the Jahn–Teller Effect. *J. Phys. Chem. Lett.* **2015**, *6*, 2657–2662.
- (60) Marelus, J.; Kolmodin, K.; Feierberg, I.; Åqvist, J. Q: A Molecular Dynamics Program for Free Energy Calculations and Empirical Valence Bond Simulations in Biomolecular Systems. *J. Mol. Graph. Model.* **1998**, *16*, 213–225.
- (61) Ryckaert, J.-P.; Ciccotti, G.; Berendsen, H. J. C. Numerical-Integration of Cartesian Equations of Motion of a System with Constraints - Molecular-Dynamics of *N*-Alkanes. *J. Comput. Phys.* **1977**, *23*, 327–341.
- (62) Berendsen, H. J. C.; Postma, J. P. M.; van Gunsteren, W. F.; DiNola, A.; Haak, J. R. Molecular Dynamics with Coupling to an External Bath. *J. Chem. Phys.* **1984**, *81*, 3684–3690.
- (63) van Der Spoel, D.; Lindahl, E.; Hess, B.; Groenhof, G.; Mark, A. E.; Berendsen, H. J. C. GROMACS: Fast, Flexible, and Free. *J. Comput. Chem.* **2005**, *26*, 1701–1718.
- (64) Noyes, R. M. Thermodynamics of Ion Hydration as a Measure of Effective Dielectric Properties of Water. *J. Am. Chem. Soc.* **1962**, *84*, 513–522.
- (65) Duarte, F.; Bauer, P.; Barrozo, A.; Amrein, B. A.; Purg, M.; Åqvist, J.; Kamerlin, S. C. L. Force Field Independent Metal Parameters Using a Nonbonded Dummy Model. *J. Phys. Chem. B* **2014**, *118*, 4351–4362.
- (66) King, G.; Warshel, A. A Surface Constrained All-Atom Solvent Model for Effective Simulations of Polar Solutions. *J. Chem. Phys.* **1989**, *91*, 3647–3661.
- (67) Lee, F. S.; Warshel, A. A Local Reaction Field Method for Fast Evaluation of Long-Range Electrostatic Interactions in Molecular Simulations. *J. Chem. Phys.* **1992**, *97*, 3100–3107.
- (68) Humphrey, W.; Dalke, A.; Schulten, K. VMD: Visual Molecular Dynamics. *J. Mol. Graph.* **1996**, *14*, 33–38.
- (69) Schrödinger Release 2016-3: MacroModel; Schrödinger, LLC: New York, NY, 2016.
- (70) Case, D.; Berryman, J. T.; Betz, R. M.; Cerutti, D. S.; Cheatham, T. E., III; Darden, T. A.; Duke, R. E.; Giese, T. J.; Gohlke, H.; Goetz, A. W.; Homeyer, N.; Izadi, S.; Janowski, P.; Kaus, J.; Kovalenko, A.; Lee, T. S.; LeGrand, S.; Li, P.; Luchko, T.; Luo, R.; Madej, B.; Merz, K. M.; Monard, G.; Needham, P.; Nguyen, H.; Nguyen, H. T.; Omelyan, I.; Onufriev, A.; Roe, D. R.; Roitberg, A.; Salomon-Ferrer, R.; Simmerling, C. L.; Smith, W.; Swails, J.; Walker, R. C.; Wang, J.; Wolf, R. M.; Wu, X.; York, D. M.; Kollman, P. A. *Amber 15*; University of California: San Francisco, 2015.